

A Comparative Study of Boundary Control With First- and Second-Order Switching Surfaces for Buck Converters Operating in DCM

Kelvin Ka-Sing Leung, *Member, IEEE*, and Henry Shu-hung Chung, *Senior Member, IEEE*

Abstract—A performance comparison of boundary control with the first- (σ^1) and second-order (σ^2) switching surfaces for buck converters operating in discontinuous conduction mode (DCM) is presented in this paper. Performance attributes under investigation include the average output voltage, output ripple voltage, switching frequency, parametric sensitivities to the component values, and large signal characteristics. Due to the presence of the output hysteresis band, an additional switching boundary formed by the zero-inductor-current trajectory is created. This phenomenon causes a shift of the operating point in converters with σ^1 . Conversely, the operating point remains unchanged in converters with σ^2 . As well as in continuous conduction mode (CCM), σ^2 can make the converter revert to the steady-state in two switching actions in DCM and gives better static and dynamic responses than σ^1 in both CCM and DCM. Most importantly, its control law and settings are applicable for both modes. Experimental results of a prototype are found to be in good agreement with theoretical predictions.

Index Terms—Boundary control, geometric control method, first-order switching surface, second-order switching surface, state trajectory control.

I. INTRODUCTION

SWITCHING converters are a class of systems that operate by variable structure control. Among various approaches, boundary control—a geometric control method—is suitable for switching converters having time-varying circuit topology. It addresses complete operation of a converter and does not differentiate startup, transient, and steady-state modes [1]. Based on studying the trajectory families for the converter on the phase plane, a switching surface is defined to dictate the switching actions. Detailed investigations into modeling and analysis of the state trajectory movement in the boundary control of converters with the first-order switching surface (σ^1) have been carried out in [1]–[8]. In general, σ^1 -derived boundary controllers offer good large signal response and stability to the converter system, but the transient dynamics is still nonoptimal. Much research work extends the concepts, such as the adaptive hysteresis control in [9] and [10], to enhance the dynamics. However, many

of them are only applicable for converters operating in continuous conduction mode (CCM). When a converter is in discontinuous conduction mode (DCM), an additional boundary due to the zero inductor current is created inherently. An unstable combination or limit cycle may emerge. Moreover, the hysteresis band causes undesirable output steady-state error.

The concept of the second-order switching surface (σ^2) is proposed in [11]–[13]. It is derived by estimating the state trajectory movement after a switching action, resulting in a high state trajectory velocity along the switching surface. This phenomenon accelerates the trajectory moving towards the target operating point. Converters with σ^2 exhibit better dynamic characteristics than the ones with σ^1 . Instead of directing the state trajectory movement, as in σ^1 , the proposed surface is derived from the natural movement of the state trajectory after a switching action. The goal is to make the converter revert to the steady state in two switching actions under large signal disturbances. The same control law and settings are equally applicable for converters operating in DCM.

Much research done on boundary control of buck converters has focused on the behaviors of converters operating in CCM. The hysteresis band is usually assumed to be zero in the analyses. There is limited information on studying the characteristics of the converters in DCM. The critical resistances of the buck converters with σ^1 and σ^2 theoretically tend to infinity with zero hysteresis band and thus DCM does not occur for a large signal stable switching surface. However, the switching frequency will also tend to infinity. Thus, a hysteresis band will usually be introduced to limit the switching frequency. With nonzero hysteresis band, an additional switching boundary formed by zero-inductor-current trajectory is created and possibly makes the converter enter into DCM. Fig. 1(a) depicts the state trajectories and Fig. 1(b) shows the time-domain output voltage and inductor current waveforms of converters in DCM with σ^1 . The output capacitor discharges to the load and the trajectory will move along the x -axis, when the main switch and the diode are off from t_2 to t_3 . This results in a shift of the average output voltage. Fig. 2(a) illustrates the output voltage shift when the output load is changed from R_1 to R_2 , where $R_2 > R_{\text{crit}}^{(1)} > R_1$ and $R_{\text{crit}}^{(1)}$ is the critical resistance. The operating point is shifted from “ O_1 ” (when the load is R_1) to a new operating point “ O_2 ” (when the load is R_2). When the load is R_1 , the converter is in CCM and the average output voltage is close to the reference voltage v_{ref} . However, when the load is R_2 , the average output will move away from “ O_1 .” For converters with σ^2 , the operating point remains unchanged.

Manuscript received April 28, 2005; revised May 25, 2006. This work was supported by the Research Grants Council of the Hong Kong Special Administrative Region, China under Project CityU 1129/05. Recommended for publication by Associate Editor D. Maksimovic.

K. K.-S. Leung is with the MKS Instruments (HK) Limited, Hong Kong (e-mail: Kelvin_Leung@mksinst.com).

H. S.-h. Chung is with the Department of Electronic Engineering, City University of Hong Kong, Kowloon, Hong Kong (e-mail: eeshc@cityu.edu.hk).

Digital Object Identifier 10.1109/TPEL.2007.900549

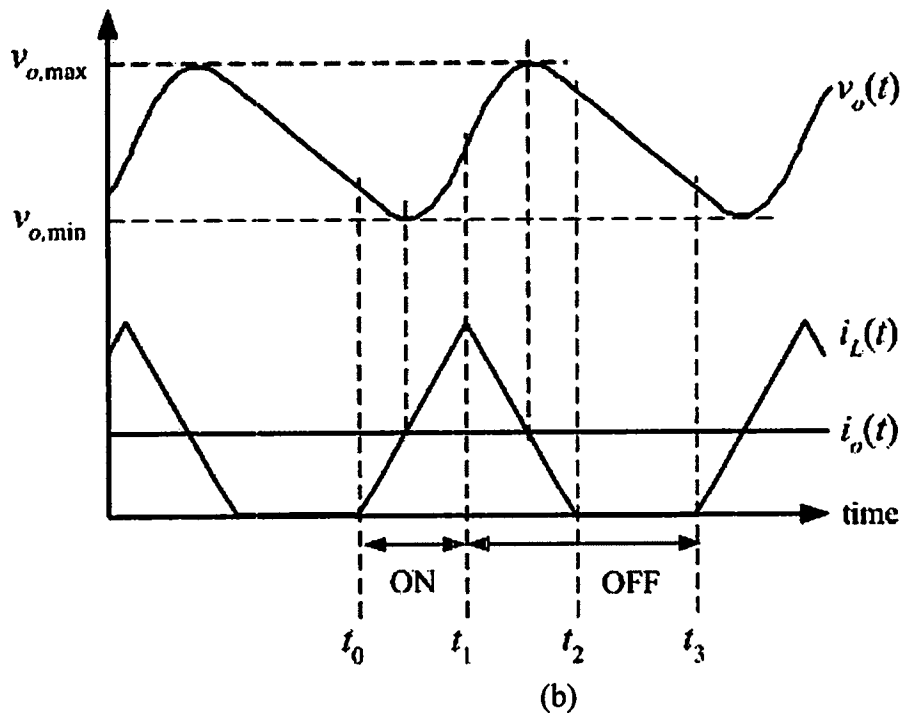
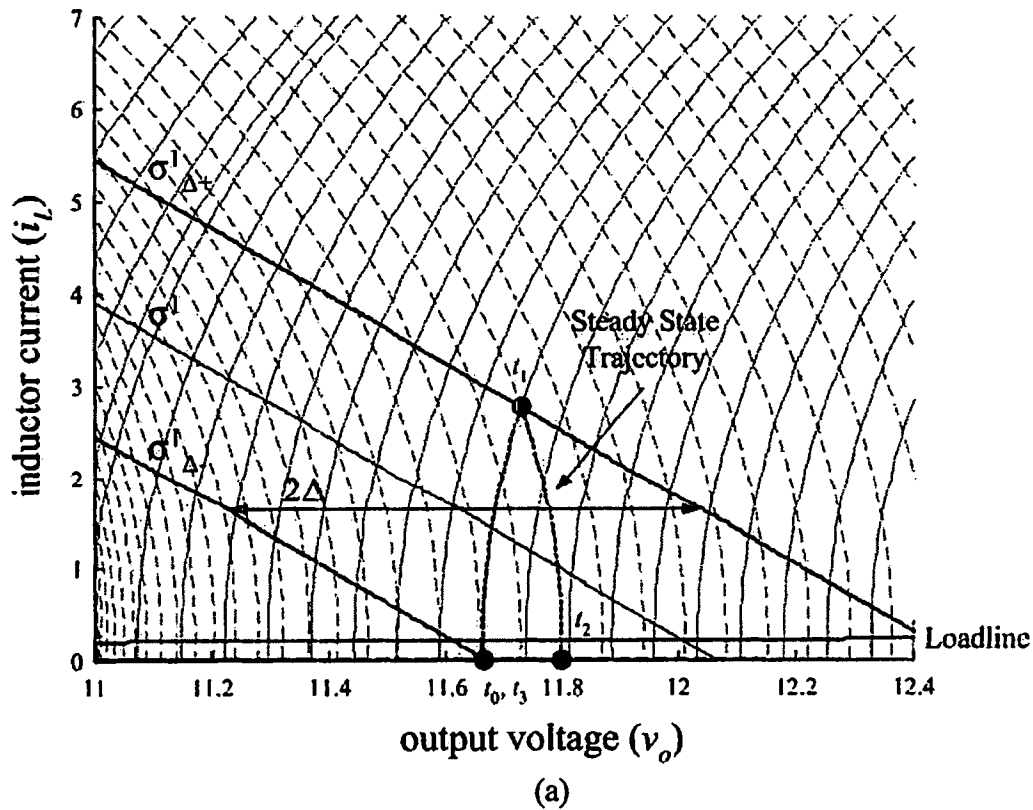


Fig. 1. Phase-plane and waveforms of the buck converter in DCM. (a) State trajectories with nonzero hysteresis band. (b) Time-domain output voltage and inductor current waveforms.

Fig. 2(b) shows the state trajectories when the load is changed from R_1 to R_2 . In this respect, σ^2 exhibits a better static behavior than σ^1 .

This paper gives a performance comparison of boundary control with σ^1 and σ^2 for buck converters operating in DCM. Performance attributes under investigation include the average

output voltage, output ripple voltage, switching frequency, parametric sensitivities to the component values, and large signal characteristics. The equivalent series resistance of the output capacitor on affecting the operating mode will also be discussed. It will be shown that σ^2 provides better dynamic responses than σ^1 for converters operating in both CCM and DCM. Ideally, the

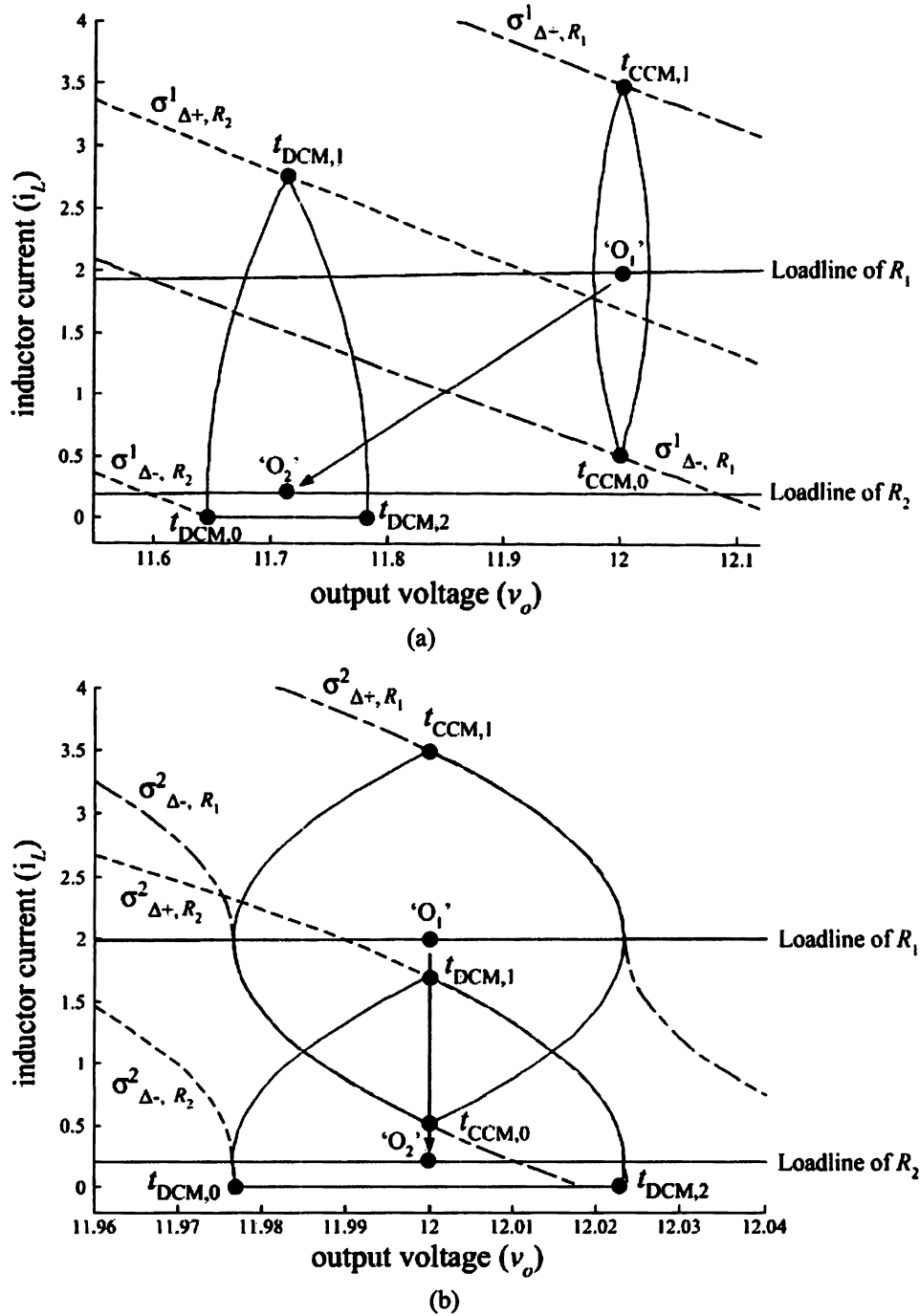


Fig. 2. Shift of operating point of the converter in DCM with different loads. (a) σ^1 . (b) σ^2 .

converter can revert to the steady state in two switching actions under large signal disturbances. Most importantly, the control law and setting of σ^2 are applicable both modes. The theoretical predictions are verified with experimental results of a prototype.

II. DEFINITIONS AND FORMULAS

The converter can be described by the state-space equation of

$$\begin{aligned} \dot{x} &= A_0x + B_0u + (A_1x + B_1u)q_1 + (A_2x + B_2u)q_2 \\ y &= Cx \end{aligned} \quad (1)$$

where $x = [i_L \ v_C]$, $y = v_o$, A_i , B_i , and C are constant matrices, and q_i represents the state of the switch S_i . If S_i is on, $q_i = 1$, and vice versa. S_1 and S_2 represent the switch and diode, respectively. Matrices A_0 , B_0 , A_1 , B_1 , A_2 , and B_2 are

$$\begin{aligned} A_0 &= \begin{bmatrix} 0 & 0 \\ 0 & -\frac{1}{C(R+r_C)} \end{bmatrix} & B_0 &= \begin{bmatrix} 0 \\ 0 \end{bmatrix} \\ A_1 = A_2 &= \begin{bmatrix} -\frac{Rr_C}{L(R+r_C)} & -\frac{R}{L(R+r_C)} \\ \frac{R}{C(R+r_C)} & 0 \end{bmatrix} \\ B_1 &= \begin{bmatrix} \frac{1}{L} \\ 0 \end{bmatrix} & B_2 &= \begin{bmatrix} 0 \\ 0 \end{bmatrix} & C &= \left[\frac{Rr_C}{R+r_C} \quad \frac{R}{R+r_C} \right]. \end{aligned}$$

A. On- and Off-State Trajectories

When S_1 is on and S_2 is off, the on-state trajectory $\{v_{o,on}, i_{L,on}\}$ is

$$v_{o,on} = \frac{L}{2C(v_i - v_{ref})} \left(\left(i_{L,on} - \frac{v_{o,on}}{R} \right)^2 - \left(i_{L,0} - \frac{v_{o,0}}{R} \right)^2 \right) + v_{o,0} + r_C \left(\left(i_{L,on} - \frac{v_{o,on}}{R} \right) - \left(i_{L,0} - \frac{v_{o,0}}{R} \right) \right) \quad (2)$$

where $i_{L,0}$ and $v_{o,0}$ are the initial values of i_L and v_o , respectively, in this stage.

When S_1 is off and S_2 is on, the off-state trajectory $\{v_{o,off}, i_{L,off}\}$ is

$$v_{o,off} = -\frac{L}{2Cv_{ref}} \left(\left(i_{L,off} - \frac{v_{o,off}}{R} \right)^2 - \left(i_{L,1} - \frac{v_{o,1}}{R} \right)^2 \right) + v_{o,1} + r_C \left(\left(i_{L,off} - \frac{v_{o,off}}{R} \right) - \left(i_{L,1} - \frac{v_{o,1}}{R} \right) \right) \quad (3)$$

where $i_{L,1}$ and $v_{o,1}$ are the initial values of i_L and v_o , respectively, in this stage.

When both S_1 and S_2 are off, the trajectory moves along the x -axis and $i_L = 0$.

B. Modeling of σ^1 and σ^2

As discussed in [13], the general form of σ^1 can be written as

$$\sigma_{\Delta+}^1 = c_1 \left(i_L - \frac{v_o}{R} \right) + (v_o - (v_{ref} + \Delta_1)) = 0 \quad (4)$$

$$\sigma_{\Delta-}^1 = c_1 \left(i_L - \frac{v_o}{R} \right) + (v_o - (v_{ref} - \Delta_1)) = 0 \quad (5)$$

where c_1 is a constant and v_{ref} is the reference output. i_L and v_o are in a linear relationship.

As discussed in [11]–[13], the general form of σ^2 is defined as

$$\sigma_{\Delta+}^2 = k_1 \left(i_L - \frac{v_o}{R} \right)^2 + (v_o - (v_{ref} + \Delta_2)), \quad \left(i_L - \frac{v_o}{R} \right) > 0 \quad (6)$$

$$\sigma_{\Delta-}^2 = -k_2 \left(i_L - \frac{v_o}{R} \right)^2 + (v_o - (v_{ref} - \Delta_2)), \quad \left(i_L - \frac{v_o}{R} \right) < 0 \quad (7)$$

where k_1 and k_2 are constants.

If $r_C = 0$, the ideal values of k_1 and k_2 are

$$\{k_1, k_2\} = \left\{ \frac{L}{2Cv_{ref}}, \frac{L}{2C(v_i - v_{ref})} \right\} \quad (8)$$

C. Average Output Voltage v_{avg} and Output Ripple Voltage

v_{ripple}

v_{avg} and v_{ripple} are defined as the mean and the difference of the minimum output voltage $v_{o,min}$ and the maximum output voltage $v_{o,max}$, respectively. That is

$$v_{avg} = \frac{v_{o,min} + v_{o,max}}{2} \quad (9)$$

$$v_{ripple} = v_{o,max} - v_{o,min} \quad (10)$$

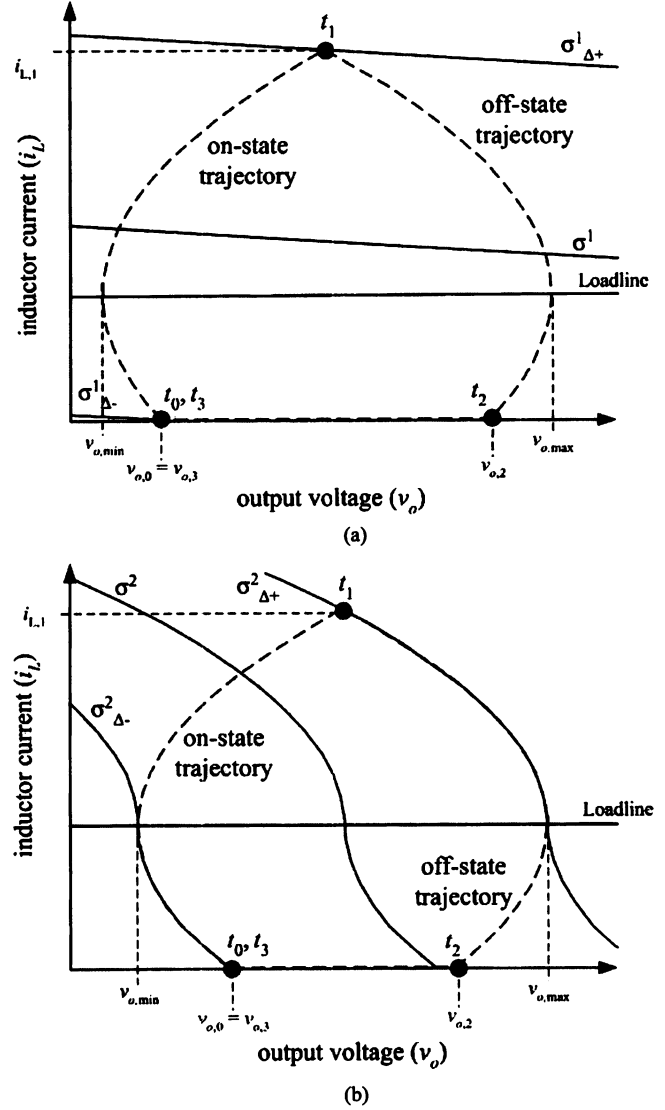


Fig. 3. Steady-state trajectories in DCM. (a) σ^1 . (b) σ^2 .

III. STEADY-STATE CHARACTERISTICS

Fig. 3(a) and (b) shows the trajectory with σ^1 and σ^2 in DCM, respectively, with $r_C = 0$

$$v_{o,0} = v_{o,3} \quad (11)$$

$$i_{L,0} = i_{L,3} \quad (12)$$

where $v_o(t_0) = v_{o,0}$, $v_o(t_3) = v_{o,3}$, $i_L(t_0) = i_{L,0}$ and $i_L(t_3) = i_{L,3}$.

In DCM, both S_1 and S_2 are off from t_2 to t_3 , therefore

$$i_{L,0} = i_{L,2} = i_{L,3} = 0 \quad (13)$$

where $i_L(t_2) = i_{L,2}$.

By putting (11)–(13) into (2)

$$v_{o,1} = \frac{L}{2C(v_i - v_{ref})} \left(\left(i_{L,1} - \frac{v_{o,1}}{R} \right)^2 - \left(\frac{v_{o,0}}{R} \right)^2 \right) + v_{o,0} \quad (14)$$

where $v_o(t_1) = v_{o,1}$, $i_L(t_1) = i_{L,1}$.

Similarly, by putting (11)–(13) into (3)

$$v_{o,2} = -\frac{L}{2Cv_{\text{ref}}} \left(\left(\frac{v_{o,2}}{R} \right)^2 - \left(i_{L,1} - \frac{v_{o,1}}{R} \right)^2 \right) + v_{o,1} \quad (15)$$

where $v_o(t_2) = v_{o,2}$.

A. Average Output Voltage and Output Ripple Voltage

1) σ^1 : As shown in [13], the converter is in critical mode, when

$$R = R_{\text{crit}}^{(1)} = \frac{v_{\text{ref}}c_1}{\Delta_1} \quad (16)$$

where $R_{\text{crit}}^{(1)}$ is the critical load resistance for $r_C = 0$.

By putting (13) into (4) and (5), they give

$$\sigma_{\Delta+}^1 = c_1 \left(i_{L,1} - \frac{v_{o,1}}{R} \right) + (v_{o,1} - (v_{\text{ref}} + \Delta_1)) = 0 \quad (17)$$

$$\sigma_{\Delta-}^1 = c_1 \left(-\frac{v_{o,0}}{R} \right) + (v_{o,0} - (v_{\text{ref}} - \Delta_1)) = 0. \quad (18)$$

By rearranging (18)

$$v_{o,0} = \frac{R}{R - c_1} (v_{\text{ref}} - \Delta_1). \quad (19)$$

By using (17) and (19) to solve (14)

$$v_{o,1} = v_{\text{ref}} + \Delta_1 - \Psi_1 \quad (20)$$

where

$$\begin{aligned} \Psi_1 &= \frac{\sqrt{1 + 8\alpha\Delta_1 - 4\Phi_1\alpha} - 1}{2\alpha} \\ \Phi_1 &= \frac{c_1}{R - c_1} (v_{\text{ref}} - \Delta_1) \left(1 - \frac{c_1\alpha(v_{\text{ref}} - \Delta_1)}{R - c_1} \right) \\ \alpha &= \frac{L}{2Cc_1^2(v_i - v_{\text{ref}})}. \end{aligned}$$

By substituting (20) into (17), it can be shown that

$$i_{L,1} = \frac{v_{\text{ref}} + \Delta_1 - \Psi_1}{R} + \frac{\Psi_1}{c_1}. \quad (21)$$

By substituting (20) and (21) into (15), equation (22), shown at the bottom of the page, can be illustrated.

As shown in [13, eq. (25) and (27)], $v_{o,\text{max}}$ and $v_{o,\text{min}}$ can be derived as

$$v_{o,\text{max}} = v_{o,1} + \frac{L}{2Cv_{\text{ref}}} \left(i_{L,1} - \frac{v_{o,1}}{R} \right)^2 \quad (23)$$

$$v_{o,\text{min}} = v_{o,0} - \frac{L}{2C(v_i - v_{\text{ref}})} \left(i_{L,0} - \frac{v_{o,0}}{R} \right)^2. \quad (24)$$

By using (20) and (21), (23) can be expressed as

$$v_{o,\text{max}} = v_{\text{ref}} - \Delta_1 + \Phi_1 + \frac{v_i\alpha}{v_{\text{ref}}}\Psi_1^2. \quad (25)$$

By using (13) and (19), (24) can be expressed as

$$v_{o,\text{min}} = v_{\text{ref}} - \Delta_1 + \Phi_1. \quad (26)$$

Thus, by putting (25) and (26) into (9)

$$v_{\text{avg}} = v_{\text{ref}} - \Delta_1 + \Phi_1 + \frac{v_i\alpha}{2v_{\text{ref}}}\Psi_1^2. \quad (27)$$

Thus, the value of v_{avg} with σ^1 is dependent on Δ_1 .

By putting (25) and (26) into (10), it can be shown that

$$v_{\text{ripple}} = \frac{v_i\alpha}{v_{\text{ref}}}\Psi_1^2. \quad (28)$$

When $R \rightarrow \infty$ and $\Phi_1 \rightarrow 0$

$$v_{\text{avg}} = v_{\text{ref}} - \Delta_1 + \frac{v_i}{8v_{\text{ref}}\alpha} (\sqrt{1 + 8\alpha\Delta_1} - 1)^2 \quad (29)$$

$$v_{\text{ripple}} = \frac{v_i}{4v_{\text{ref}}\alpha} (\sqrt{1 + 8\alpha\Delta_1} - 1)^2. \quad (30)$$

2) σ^2 : As shown in [13], the converter is in critical mode, when

$$R = R_{\text{crit}}^{(2)} = \frac{v_{\text{ref}} - \frac{k_1 - k_2}{k_1 + k_2}\Delta_2}{\sqrt{\frac{2\Delta_2}{k_1 + k_2}}} \quad (31)$$

where $R_{\text{crit}}^{(2)}$ is the critical load resistance for $r_C = 0$.

By putting (13) into (6) and (7)

$$\sigma_{\Delta+}^2 = k_1 \left(i_{L,1} - \frac{v_{o,1}}{R} \right)^2 + (v_{o,1} - (v_{\text{ref}} + \Delta_2)) = 0 \quad (32)$$

$$\sigma_{\Delta-}^2 = -k_2 \left(\frac{v_{o,0}}{R} \right)^2 + (v_{o,0} - (v_{\text{ref}} - \Delta_2)) = 0. \quad (33)$$

By solving (33) for $v_{o,0}$, it gives

$$v_{o,0} = \frac{R^2}{2k_2} \left(1 - \sqrt{1 - \frac{4k_2}{R^2}(v_{\text{ref}} - \Delta_2)} \right). \quad (34)$$

$$v_{o,2} = \frac{CR^2v_{\text{ref}}}{L} \left(-1 + \sqrt{1 + \frac{2L}{CR^2v_{\text{ref}}} \left(v_{\text{ref}} + \Delta_1 - \Psi_1 + \frac{L}{2Cc_1^2v_{\text{ref}}}\Psi_1^2 \right)} \right). \quad (22)$$

By solving (14) with (32) and (34), it gives

$$v_{o,1} = v_{\text{ref}} + \Delta_2 - \Psi_2 \quad (35)$$

where

$$\begin{aligned} \Psi_2 &= \frac{2\Delta_2 - \Phi_2}{1 + \beta} \\ \Phi_2 &= (k_2 - \beta k_1) \left(\frac{R}{2k_2} \left(1 - \sqrt{1 - \frac{4k_2}{R^2} (v_{\text{ref}} - \Delta_2)} \right) \right)^2 \\ \beta &= \frac{L}{2Ck_1(v_i - v_{\text{ref}})}. \end{aligned}$$

By substituting (35) into (32), it can shown that

$$i_{L,1} = \frac{v_{\text{ref}} + \Delta_2 - \Psi_2}{R} + \sqrt{\frac{\Psi_2}{k_1}}. \quad (36)$$

By substituting (35) and (36) into (15), equation (37), shown at the bottom of the page, is illustrated.

By using (35) and (36), (23) can be expressed as

$$v_{o,\max} = v_{\text{ref}} - \Delta_2 + \Phi_2 + \frac{v_i \beta}{v_{\text{ref}}} \Psi_2. \quad (38)$$

By using (13) and (34), (24) can be expressed as

$$v_{o,\min} = v_{\text{ref}} - \Delta_2 + \Phi_2. \quad (39)$$

By substituting (38) and (39) into (9), it can shown that

$$v_{\text{avg}} = v_{\text{ref}} - \Delta_2 + \Phi_2 + \frac{v_i \beta}{2v_{\text{ref}}} \Psi_2. \quad (40)$$

By putting (38) and (39) into (10)

$$v_{\text{ripple}} = \frac{v_i \beta}{v_{\text{ref}}} \Psi_2. \quad (41)$$

When $R \rightarrow \infty$ and $\Phi_2 \rightarrow 0$

$$v_{\text{avg}} = v_{\text{ref}} - \Delta_2 + \frac{\beta}{1 + \beta} \frac{v_{\text{in}}}{v_{\text{ref}}} \Delta_2 \quad (42)$$

$$v_{\text{ripple}} = \frac{2\beta}{1 + \beta} \frac{v_i}{v_{\text{ref}}} \Delta_2. \quad (43)$$

With the ideal values of k_1 and k_2 in (8)

$$v_{\text{avg}} = v_{\text{ref}} \quad (44)$$

$$v_{\text{ripple}} = 2\Delta_2 \quad (45)$$

for $R > R_{\text{crit}}^{(2)}$. It can be noted that v_{avg} is independent on Δ_2 .

B. Switching Frequency

In DCM, $i_{L,0} = i_{L,2} = i_{L,3} = 0$ and $v_{o,0} = v_{o,3}$. With $r_C = 0$, the average output current I_o can be expressed as

$$\begin{aligned} I_o &= \bar{i}_L = \frac{1}{T_S} \int_{t_0}^{t_3} i_L dt \\ &= \frac{1}{T_S} \left(\int_{t_0}^{t_1} i_L dt + \int_{t_1}^{t_2} i_L dt + \int_{t_2}^{t_3} i_L dt \right) \end{aligned} \quad (46)$$

$$\begin{aligned} I_o &= \frac{1}{T_S} \left(\int_{i_{L,0}}^{i_{L,1}} \frac{Li_L}{v_i - v_{\text{ref}}} di_L \right. \\ &\quad \left. + \int_{i_{L,1}}^{i_{L,2}} \frac{-Li_L}{v_{\text{ref}}} di_L + \int_{i_{L,2}}^{i_{L,3}} 0 di_L \right) \\ &= \frac{1}{T_S} \frac{Lv_i i_{L,1}^2}{2v_{\text{ref}}(v_i - v_{\text{ref}})}. \end{aligned} \quad (47)$$

Therefore, the switching frequency f_S can be expressed as

$$f_S = \frac{1}{T_S} = \frac{2v_{\text{ref}}(v_i - v_{\text{ref}})}{Lv_i i_{L,1}^2} I_o. \quad (48)$$

1) σ^1 : Thus, the switching frequency for σ^1 can be obtained by substituting (21) into (48)

$$f_S = \frac{1}{T_S} = \frac{2v_{\text{ref}}(v_i - v_{\text{ref}})}{Lv_i \left(\frac{v_{\text{ref}} + \Delta_1 - \Psi_1}{R} + \frac{\Psi_1}{c_1} \right)^2} I_o. \quad (49)$$

2) σ^2 : The switching frequency with σ^2 can be calculated by substituting (36) into (48)

$$f_S = \frac{1}{T_S} = \frac{2v_{\text{ref}}(v_i - v_{\text{ref}})}{Lv_i \left(\frac{v_{\text{ref}} + \Delta_2 - \Psi_2}{R} + \sqrt{\frac{\Psi_2}{k_1}} \right)^2} I_o. \quad (50)$$

C. Simplified Expressions of v_{avg} , v_{ripple} , and f_S

Equations (29), (30), and (49) give the expressions of v_{avg} , v_{ripple} , and f_S for converters with σ^1 , while (40), (41), and (50) give the expressions for converters with σ^2 . In order to study their relationships with I_o , some simplifications have been made in the following.

1) σ^1 : By substituting $[i_{L,0}, v_{o,0}] = [0, v_{o,\min}]$ into (5) and assuming $v_{o,\min} \approx v_{\text{avg}}$

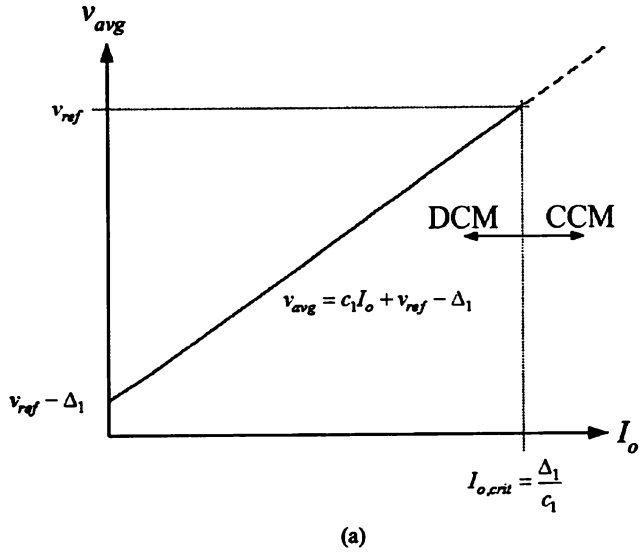
$$v_{\text{avg}} = c_1 I_o + v_{\text{ref}} - \Delta_1 \quad (51)$$

where $I_o = v_{\text{avg}}/R$.

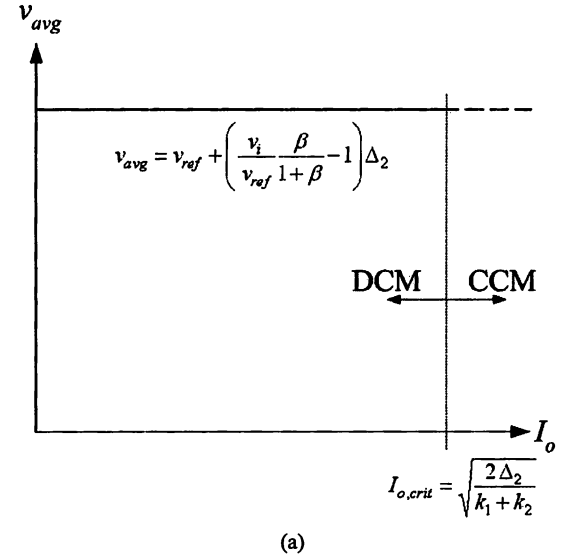
By substituting $v_{o,1}$ with v_{avg} in (20) and comparing the result with (51), it gives

$$\Psi_1 = 2\Delta_1 - c_1 I_o. \quad (52)$$

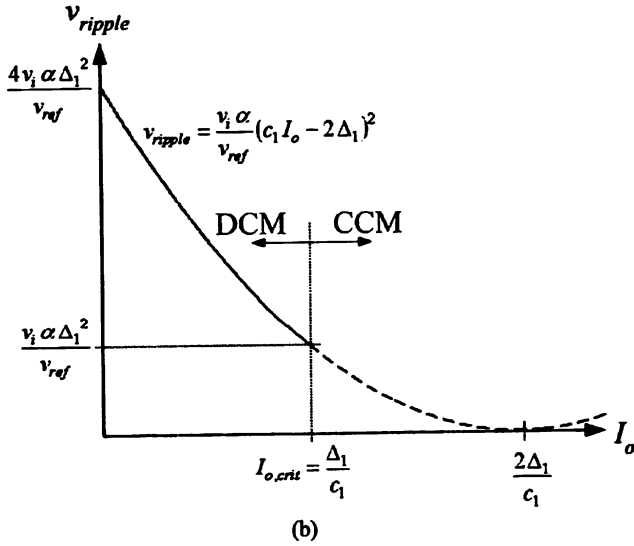
$$v_{o,2} = \frac{CR^2 v_{\text{ref}}}{L} \left(-1 + \sqrt{1 + \frac{2L}{CR^2 v_{\text{ref}}} \left(v_{\text{ref}} + \Delta_2 - \Psi_2 + \frac{L}{2Cv_{\text{ref}} k_1} \Psi_2 \right)} \right). \quad (37)$$



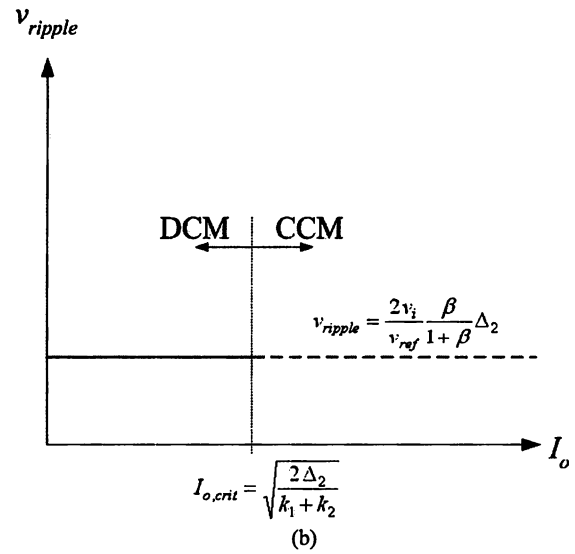
(a)



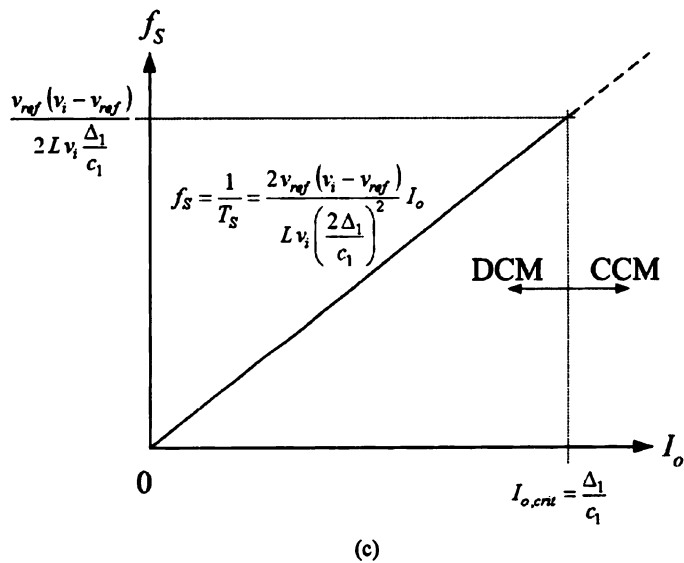
(a)



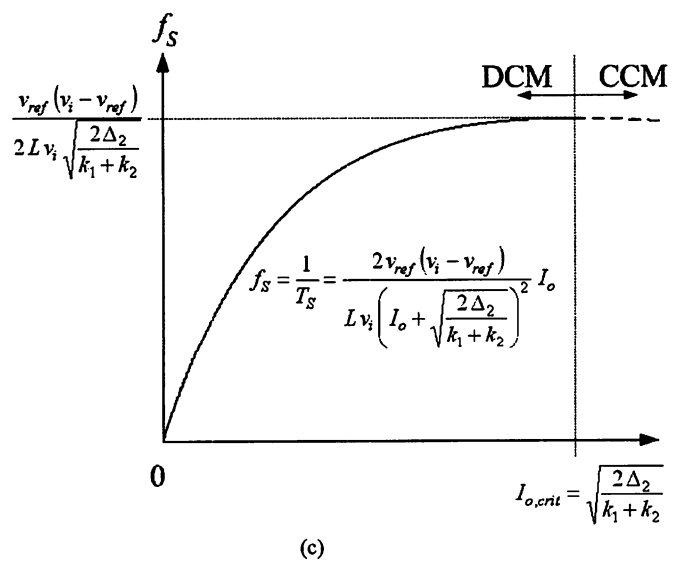
(b)



(b)



(c)



(c)

Fig. 4. Steady-state characteristics of converters with σ^1 . (a) v_{avg} . (b) v_{ripple} . (c) f_s .

Fig. 5. Steady-state characteristics of converters with σ^2 . (a) v_{avg} . (b) v_{ripple} . (c) f_s .

Then, by putting (52) into (28), it gives

$$v_{ripple} = \frac{v_i \alpha}{v_{ref}} (c_1 I_o - 2\Delta_1)^2. \quad (53)$$

By putting (20) and (52) into (21), it can be shown that

$$i_{L,1} = \frac{2\Delta_1}{c_1}. \quad (54)$$

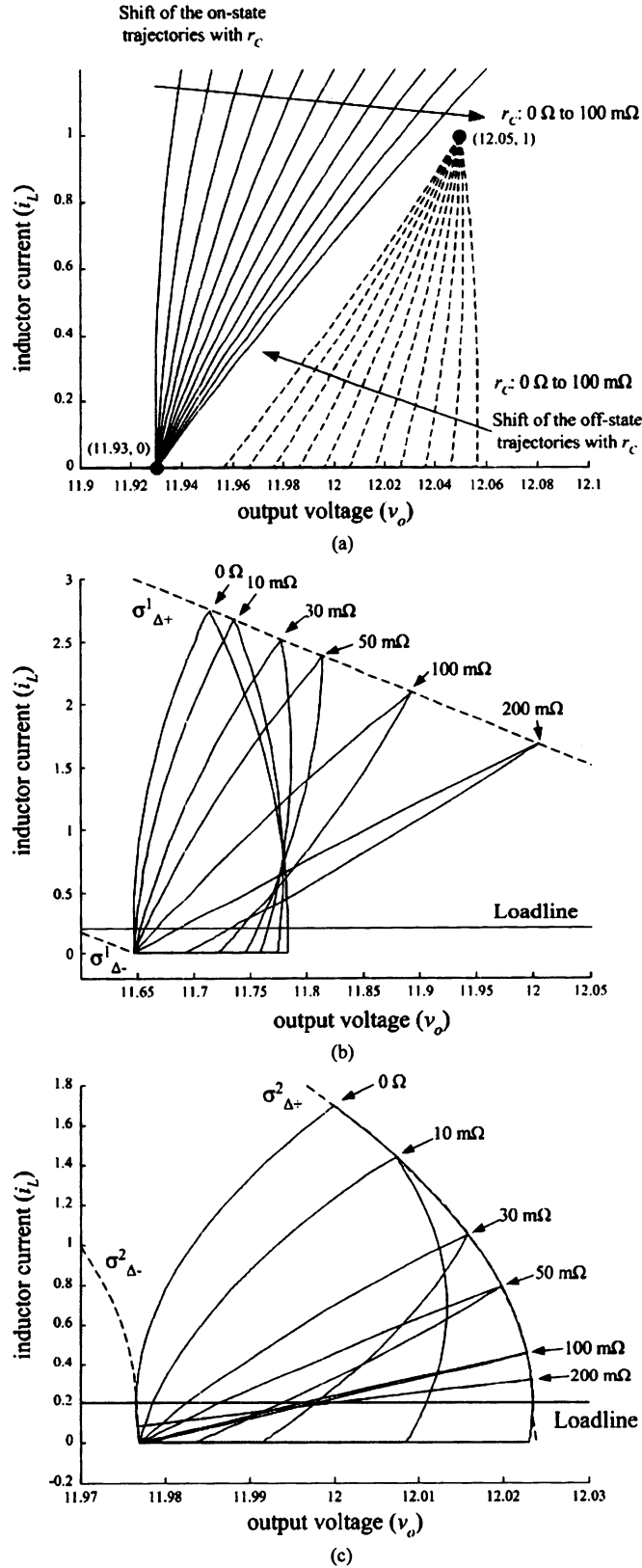


Fig. 6. Shift of steady-state trajectories against r_C . (a) The on- and off-state trajectories. (b) Converter trajectories with σ^1 . (c) Converter trajectories with σ^2 .

Thus, by substituting (54) into (48), the switching frequency can be expressed as

$$f_s = \frac{1}{T_S} = \frac{2v_{ref}(v_i - v_{ref})}{Lv_i \left(\frac{2\Delta_1}{c_1} \right)^2} I_o. \quad (55)$$

TABLE I
COMPONENT VALUES OF THE PROTOTYPE

Parameter	Value
v_i	24 V
v_{ref}	12 V
L	100 μ H
C	400 μ F
R	60 Ω
c_1	0.2702
$\{k_1, k_2\}$	$\{0.0104, 0.0104\}$
f_s	20 kHz
Δ_1	405.3 mV
Δ_2	23.4 mV

Fig. 4 shows the steady-state characteristics against the load current I_o . $I_{o,crit}$ is the value of I_o when $R = R_{crit}^{(1)}$.

2) σ^2 : For the ideal values of k_1 and k_2 in (8), $k_2 - \beta k_1 = 0 \Rightarrow \Phi_2 = 0$. Thus

$$\Psi_2 = \frac{2\Delta_2}{1 + \beta}. \quad (56)$$

By substituting $v_{o,1}$ with v_{avg} , and (35) into (36), (40), and (41), it can be shown that

$$i_{L,1} = I_o + \sqrt{\frac{2\Delta_2}{k_1(1 + \beta)}} = I_o + \sqrt{\frac{2\Delta_2}{k_1 + k_2}} \quad (57)$$

$$v_{avg} = v_{ref} + \left(\frac{v_i}{v_{ref}} \frac{\beta}{1 + \beta} - 1 \right) \Delta_2 \quad (58)$$

$$v_{ripple} = \frac{2v_i}{v_{ref}} \frac{\beta}{1 + \beta} \Delta_2. \quad (59)$$

Thus, by putting (57) into (48), the switching frequency can be expressed as

$$f_s = \frac{1}{T_S} = \frac{2v_{ref}(v_i - v_{ref})}{Lv_i \left(I_o + \sqrt{\frac{2\Delta_2}{k_1 + k_2}} \right)^2} I_o. \quad (60)$$

Fig. 5 shows the steady-state characteristics against the load current I_o .

D. Effects of r_C on the Operating Mode

As illustrated in Fig. 6(a), the on- and off-state trajectories vary with r_C . Fig. 6(b) and (c) shows the shifts of the steady-state trajectories with different values of r_C for the converter with σ^1 and σ^2 , respectively. The analyses are based on the component values tabulated in Table I. The converter changes from DCM to CCM, as r_C increases. Moreover, the steady-state on and off trajectories will move along the same path and become a straight line. Similar to the method described in [3], a straight line of slope m connecting the two switching instants t_0 and t_1 can be expressed as

$$m = \frac{i_{L,1} - i_{L,0}}{v_{o,1} - v_{o,0}} = \frac{R + r_C}{Rr_C}. \quad (61)$$

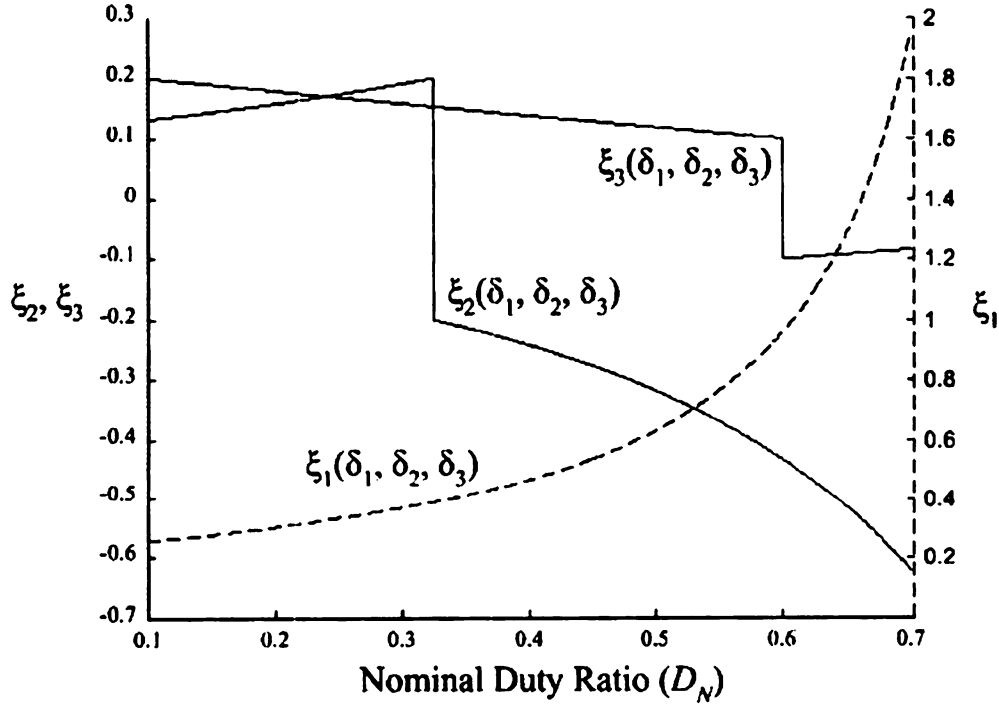


Fig. 7. Maximum values of ξ_1 , ξ_2 , and ξ_3 at different duty cycle D_N .

By putting $i_{L,0} = 0$ and assuming that the line passes through the point $\{v_{\text{ref}}, \frac{v_{\text{ref}}}{R}\}$ in CCM, (61) can be expressed as

$$r_C = \left(\frac{v_{\text{ref}}}{v_{o,0}} - 1 \right) R. \quad (62)$$

Thus, the critical value of r_C , $r_{C,\text{crit}}$, that the converter starts operating in CCM can be calculated by substituting (19) into (62) for σ^1 , and (34) into (62) for σ^2 . For σ^1

$$r_{C,\text{crit}}^{(1)} = R \left(\frac{\Delta_1}{v_{\text{ref}} - \Delta_1} \right) - c_1 \left(\frac{v_{\text{ref}}}{v_{\text{ref}} - \Delta_1} \right). \quad (63)$$

For σ^2

$$r_{C,\text{crit}}^{(2)} = \left(\frac{2k_2 v_{\text{ref}}}{R^2 \left(1 - \sqrt{1 - \frac{4k_2}{R^2} (v_{\text{ref}} - \Delta_2)} \right)} - 1 \right) R. \quad (64)$$

IV. PARAMETRIC VARIATIONS ON THE CONVERTER CHARACTERISTICS

The components L and C , and v_i are subject to variation

$$v_i = v_{i,N}(1 + \delta_1) \quad (65)$$

$$L = L_N(1 + \delta_2) \quad (66)$$

$$C = C_N(1 + \delta_3) \quad (67)$$

where $v_{i,N}$, L_N , and C_N are the nominal values of v_i , L , and C , respectively, and δ_1 , δ_2 , and δ_3 are the fractional variations of v_i , L , and C , respectively. Sensitivities of v_{avg} , v_{ripple} , and f_S to δ_1 , δ_2 , and δ_3 are based on (51), (53), and (55) for σ^1 and (58)–(60) for σ^2 .

A. With σ^1

By putting (65)–(67) into (51), (53), and (55), the percent change of v_{avg} , v_{ripple} , and f_S is

$$\% \Delta v_{\text{avg}} = \frac{v_{\text{avg}}(v_i, L, C) - v_{\text{avg}}(v_{i,N}, L_N, C_N)}{v_{\text{avg}}(v_{i,N}, L_N, C_N)} = 0 \quad (68)$$

$$\begin{aligned} \% \Delta v_{\text{ripple}} &= \frac{v_{\text{ripple}}(v_i, L, C) - v_{\text{ripple}}(v_{i,N}, L_N, C_N)}{v_{\text{ripple}}(v_{i,N}, L_N, C_N)} \\ &= \xi_1(\delta_1, \delta_2, \delta_3) \end{aligned} \quad (69)$$

$$\begin{aligned} \% \Delta f_S &= \frac{f_S(v_i, L, C) - f_S(v_{i,N}, L_N, C_N)}{f_S(v_{i,N}, L_N, C_N)} \\ &= \xi_2(\delta_1, \delta_2, \delta_3) \end{aligned} \quad (70)$$

where $D_N = v_{\text{ref}}/v_{i,N}$ is a nominal duty cycle

$$\xi_1(\delta_1, \delta_2, \delta_3) = \frac{(1 + \delta_1)(1 + \delta_2)(1 - D_N)}{(1 + \delta_3)(1 + \delta_1 - D_N)} - 1$$

and

$$\xi_2(\delta_1, \delta_2, \delta_3) = \frac{(1 + \delta_1) - D_N}{(1 + \delta_1)(1 + \delta_2)(1 - D_N)} - 1.$$

B. With σ^2

By substituting (65)–(67) into (58), (59), and (60), the percent change of v_{avg} , v_{ripple} , and f_S from its nominal value is

$$\% \Delta v_{\text{avg}} = \xi_3(\delta_1, \delta_2, \delta_3) \frac{\Delta_2}{v_{\text{ref}}} \quad (71)$$

$$\% \Delta v_{\text{ripple}} = \xi_3(\delta_1, \delta_2, \delta_3) \quad (72)$$

$$\% \Delta f_S = \xi_2(\delta_1, \delta_2, \delta_3) \quad (73)$$

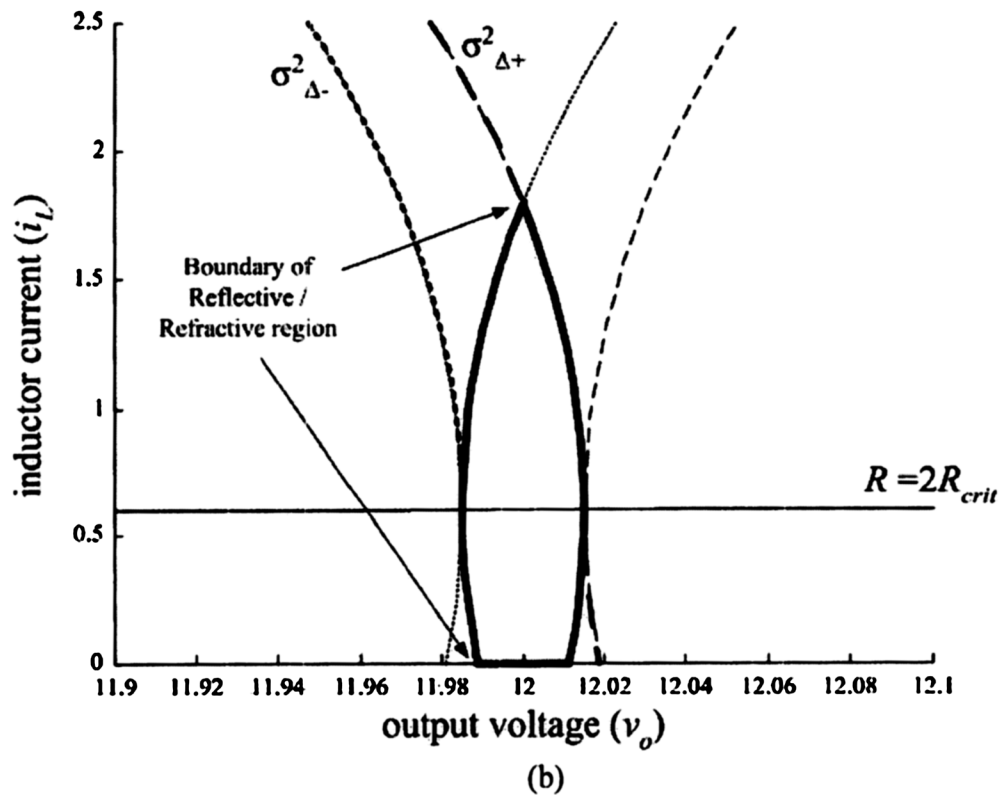
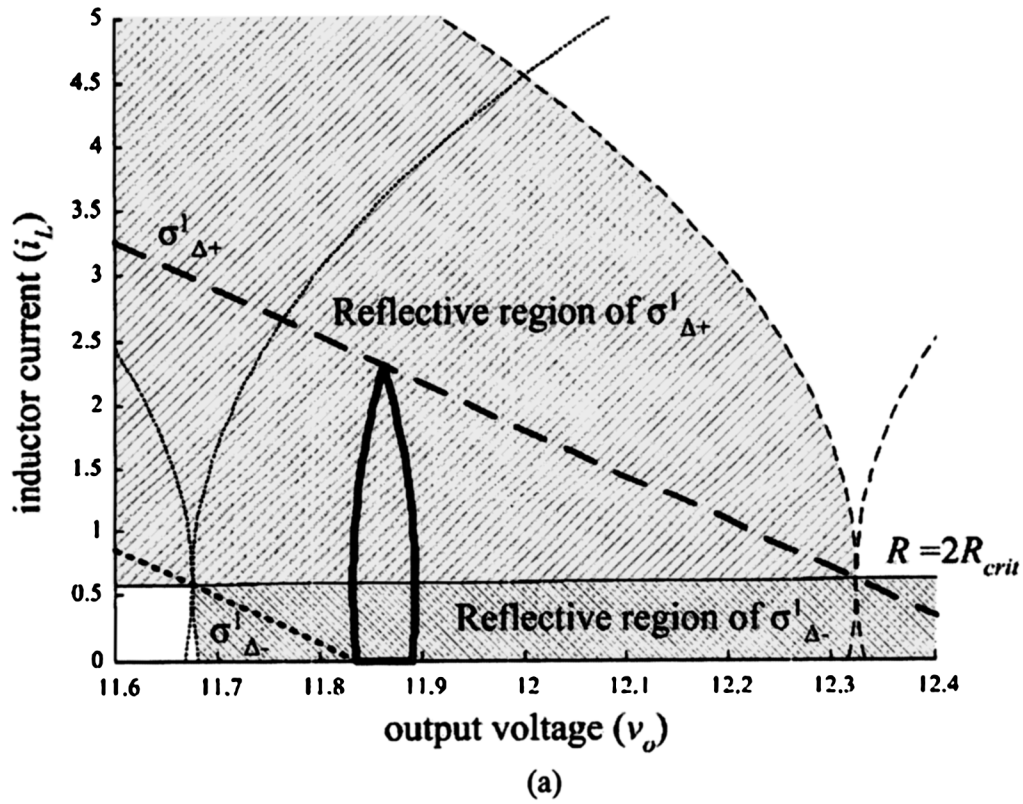


Fig. 8. Transition boundaries of the upper and lower bounds. (a) σ^1 . (b) σ^2 .

where

$$\xi_3(\delta_1, \delta_2, \delta_3) = \frac{(1 + \delta_1)(1 + \delta_2)}{(1 + \delta_1)(1 + \delta_3) + D_N(\delta_2 - \delta_3)} - 1.$$

By using the function of “fmincon” on MATLAB, Fig. 7 shows the maximum value of ξ_1, ξ_2 , and ξ_3 at different duty cycle D_N from 0.1 to 0.7, where v_i is subject to a maximum variation of $\pm 20\%$ (i.e., $\delta_1 \in [-0.2, +0.2]$), and L and C

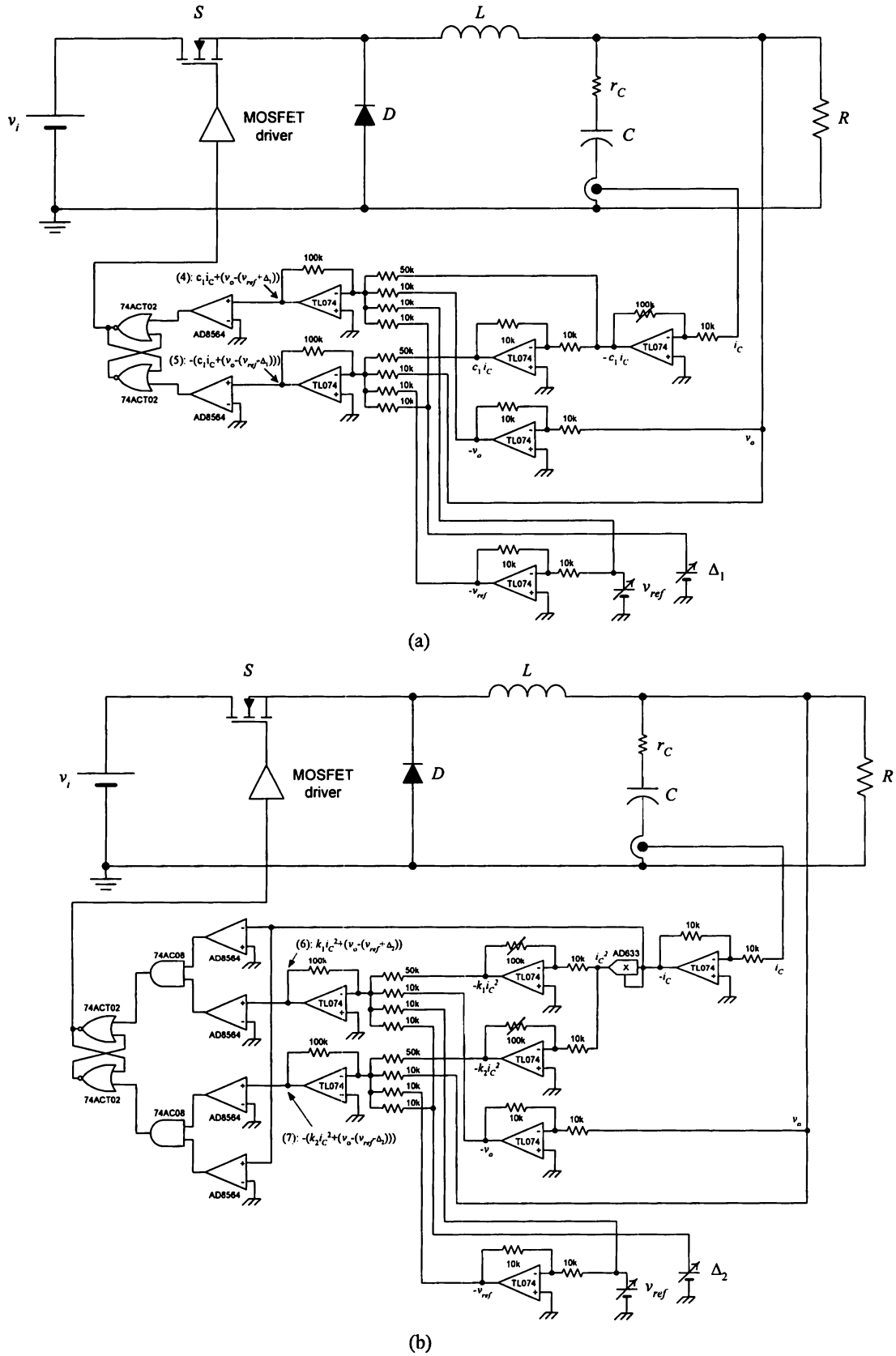
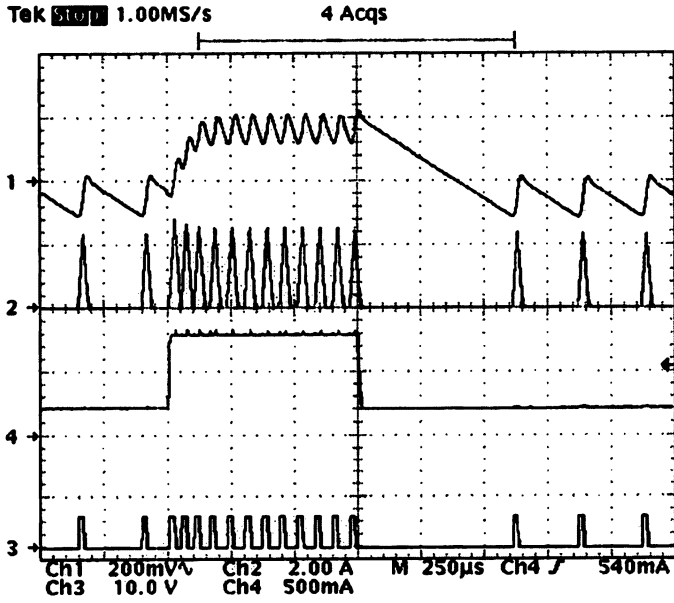


Fig. 9. Circuit implementations of the two controllers. (a) σ^1 . (b) σ^2 .

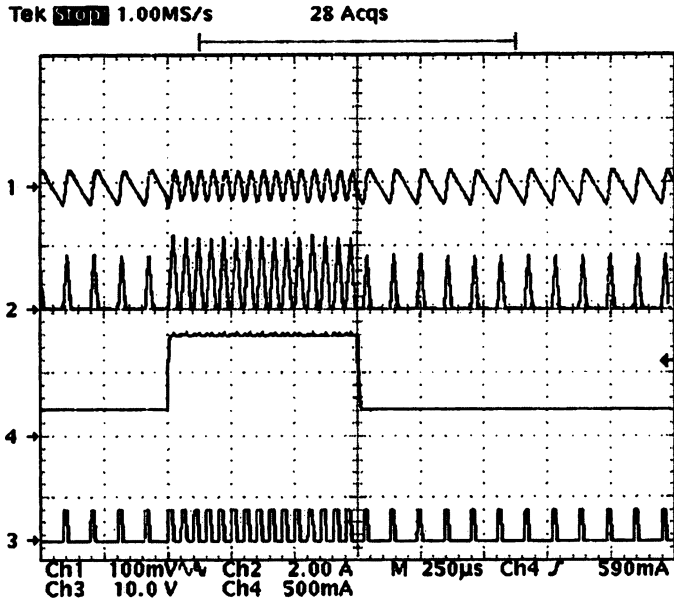
are subject to a maximum variation of $\pm 10\%$ (i.e., $\delta_2, \delta_3 \in [-0.1, +0.1]$).

The v_{avg} in σ^2 [see (71)] is sensitive to the component variation, as compared with σ^1 [see (68)]. It is mainly because

σ^2 is dependent on the component values, while σ^1 is explicitly determined. However, as shown in (71), $\Delta_2 \ll v_{ref}$, the variation of v_{avg} with respect to parametric variation is very small.



(a)



(b)

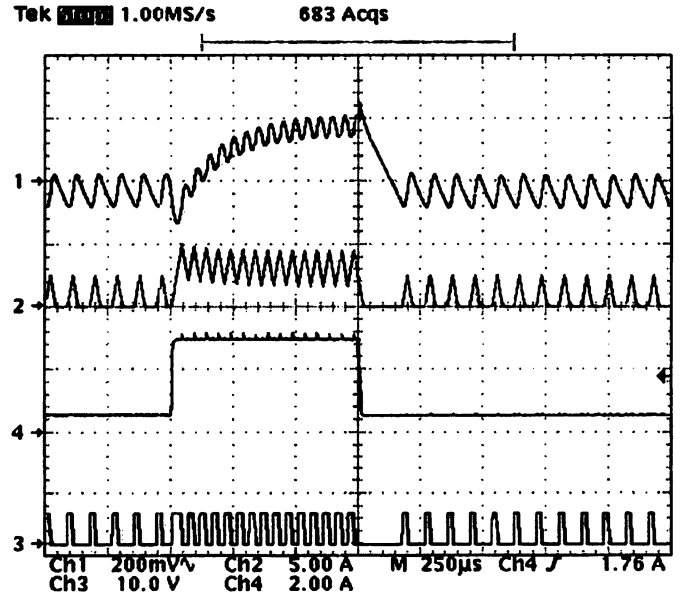
Fig. 10. Transient response of buck converter when load change from 0.2 A (2.4 W) to 0.8 A (9.6 W), and vice versa. [Ch2: i_L (2 A/div), Ch3: v_g (10 V/div), Ch4: i_o (500 mA/div)] (Timebase: 250 μ s/div). (a) σ^1 [Ch1: v_o (200 mV/div)]. (b) σ^2 [Ch1: v_o (100 mV/div)].

Comparing (69) with (72), the variation of v_{ripple} in σ^2 is much less than that of σ^1 . The former one only varies between -15% and $+20\%$, while the latter one can be up to 200%.

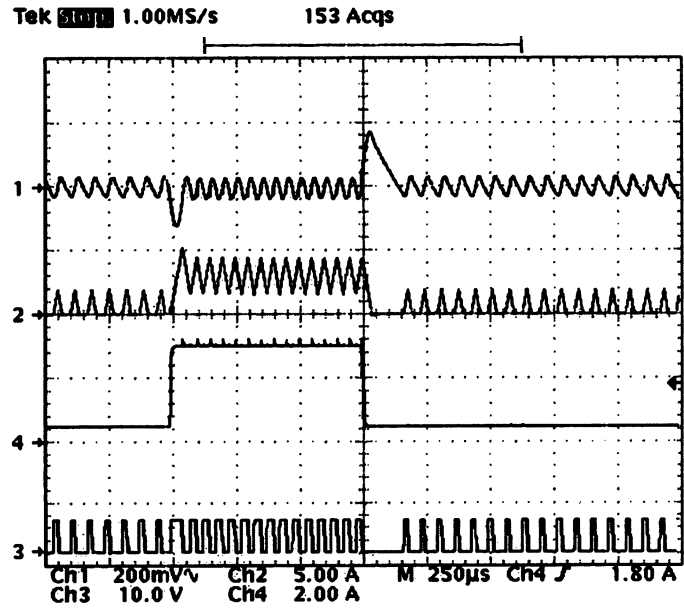
Comparing (70) with (73), the frequency variations in the two switching surfaces are the same.

V. LARGE SIGNAL CHARACTERISTICS

The large signal analysis method shown in [13] is based on assuming that the hysteresis band is zero. As DCM is introduced by nonzero hysteresis band, the large signal characteristics are studied by considering the transition boundaries of the upper and lower bounds. The transition boundaries with σ^1 and σ^2 are shown in Fig. 8. As illustrated in Fig. 8(a), the transition



(a)



(b)

Fig. 11. Transient response of buck converter when load change from 0.5 A (6 W) to 3 A (36 W), and vice versa. [Ch1: v_o (200 mV/div), Ch2: i_L (5 A/div), Ch3: v_g (10 V/div), Ch4: i_o (2 A/div)] (Timebase: 250 μ s/div). (a) σ^1 . (b) σ^2 .

boundaries for $\sigma_{\Delta-}^1$ and $\sigma_{\Delta+}^1$ are all in the reflective regions (as shown in [13, Fig. 5(a)]) and thus the converter is in the sliding mode. The transition boundaries for $\sigma_{\Delta-}^2$ and $\sigma_{\Delta+}^2$ are similar to the ones in CCM and are always on the boundaries of reflective and refractive regions [Fig. 8(b)]. It exhibits the advantages of providing near-optimum transient response to large signal disturbances.

VI. EXPERIMENTAL VERIFICATIONS

A buck converter with the component values tabulated in Table I is studied. The same power circuit is controlled by two different boundary controllers. Fig. 9(a) and (b) shows the circuit schematics of the controllers with σ^1 and σ^2 , respectively.

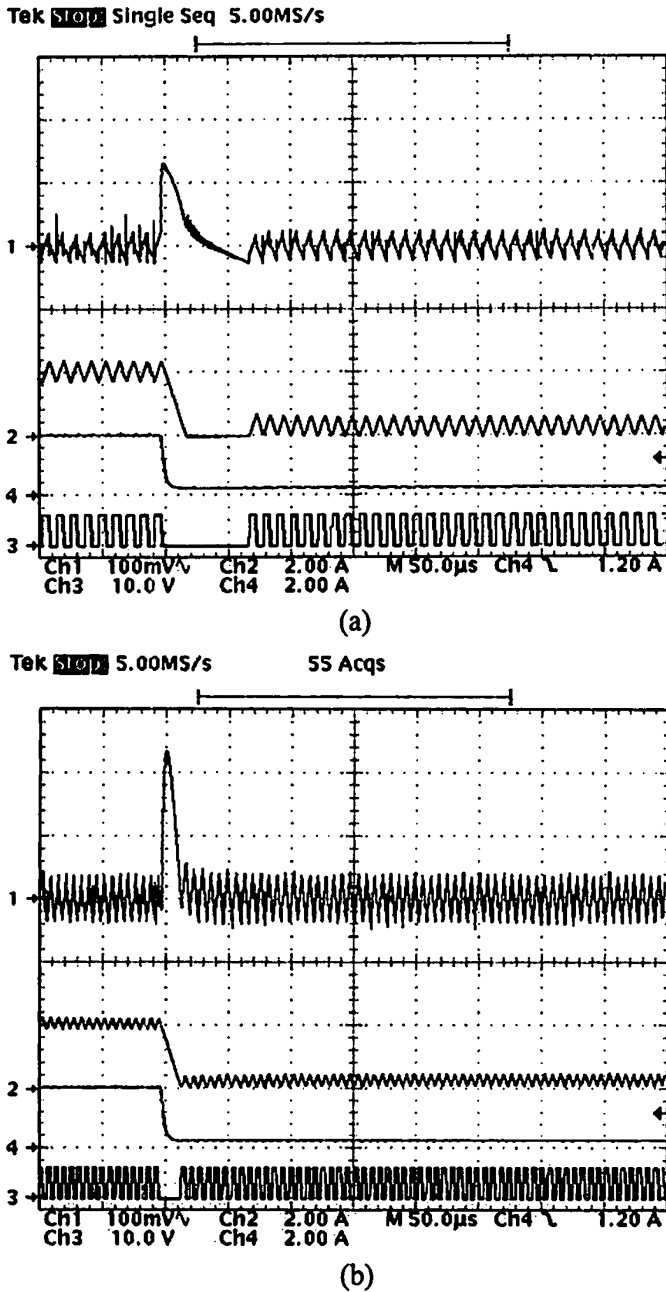


Fig. 12. Transient response of buck converter when I_o is changed from 2 A (24 W) to 0.2 A (2.4 W). [Ch1: v_o (100 mV/div), Ch2: i_L (2 A/div), Ch3: v_g (10 V/div), Ch4: i_o (2 A/div)] (Timebase: 50 μ s/div). (a) $r_C = 100$ m Ω . (b) $r_C = 200$ m Ω .

Comparing the two controllers, their only differences are the inclusions of a multiplier, several logic gates, and comparators for the switching criteria in realizing σ^2 .

The parameter c_1 in σ^1 is obtained by optimizing the startup transient as in [13]. Fig. 10 shows the transient responses with σ^1 and σ^2 , respectively, when the output load is changed from 0.2 A (2.4 W) to 0.8 A (9.6 W), and vice versa. It can be seen that the output has a voltage drift in σ^1 and does not appear in σ^2 . σ^1 takes about 200 μ s to settle, while σ^2 has virtually no transient period. Fig. 11 shows the converter response when it is subject to a large signal change that the load is changed from 0.5 A (6 W) to 3 A (36 W), and vice versa. The operating mode of the converter is switched between DCM and CCM. The converter

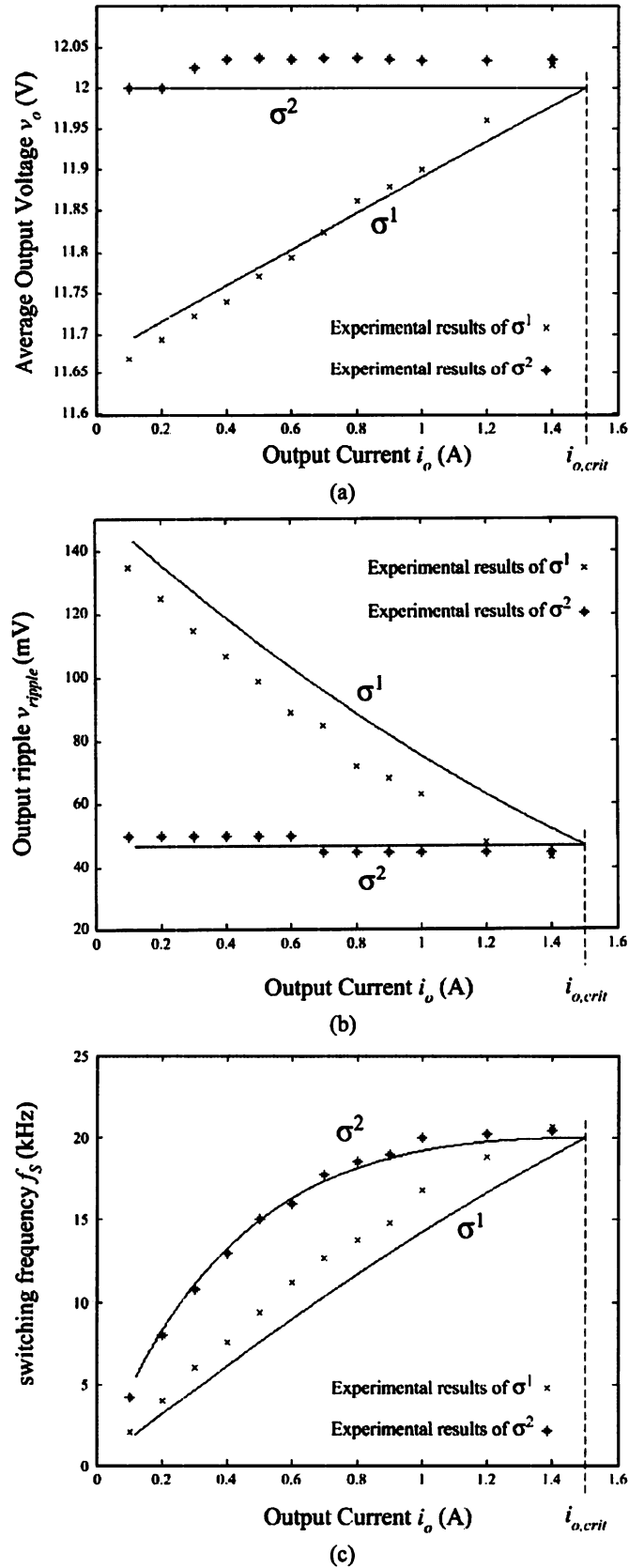


Fig. 13. Measurement results of the steady-state characteristics of converters with σ^1 and σ^2 . (a) v_{avg} . (b) v_{ripple} . (c) f_s .

with σ^1 takes more than 500 μ s to settle from 0.5 to 3 A and takes 200 μ s from 3 to 0.5 A. The one with σ^2 takes about 50 μ s to settle from 0.5 to 3 A and takes 150 μ s from 3 to 0.5 A. Thus,

σ^2 exhibits better dynamic response than σ^1 . With the same control law, the converter with σ^2 can regulate the output in both modes and there is no voltage drift. The dynamic response with σ^2 is much better than that of σ^1 . Fig. 12(a) and (b) shows the converter output with r_C equal to 100 and 200 m Ω , respectively. The output current is changed from 2 to 0.2 A. The equivalent value of R when $I_o = 0.2$ A is 60 Ω . Based on (64), $r_{C,crit}^{(2)} = 115$ m Ω . When $r_C = 100$ m Ω , the converter at $I_o = 0.2$ A is close to the critical mode [Fig. 11(a)]. When $r_C = 200$ m Ω , the converter at $I_o = 0.2$ A is in CCM [Fig. 11(b)]. This confirms the discussion in Section III. Fig. 13 shows the measurement results of v_{avg} , v_{ripple} , and f_S with σ^1 and σ^2 , as compared with (29), (30), and (49) for σ^1 and (40), (41), and (50) for σ^2 . Theoretical predictions are in good agreement with experimental results.

Based on the experimental observations, the boundary controllers with σ^2 have the following advantages over than the ones with σ^1 .

- 1) The same controller is applicable for converters operating in both CCM and DCM.
- 2) No voltage drift occurs, even if the converter is in DCM.
- 3) The dynamic response is better. The converter can ideally revert to the steady state in two switching actions.
- 4) The optimal values of the control parameters can be obtained readily by considering the component values. It is unnecessary to use a trial-and-error approach to determine the control parameters.
- 5) The ripple voltage is relatively constant over the load range with σ^2 .

Nevertheless, the advantages are at the expense of requiring more circuit components for implementing the switching criteria.

VII. CONCLUSION

A comparative study of the static and dynamic behaviors of buck converters operating in DCM with the first- and second-order switching surfaces have been examined. Detailed mathematical analyses have been given and have been supported by experimental measurements.

REFERENCES

- [1] P. T. Krein, *Elements of Power Electronics*. Oxford, U.K.: Oxford Univ. Press, 1998, ch. 17.
- [2] P. T. Krein, *Nonlinear Phenomena in Power Electronics: Attractors, Bifurcation, Chaos, and Nonlinear Control*. New York: IEEE Press, 2001, ch. 8.
- [3] R. Munzert and P. T. Krein, "Issues in boundary control," in *Proc. IEEE Power Electron. Specialists Conf.*, 1996, pp. 810–816.
- [4] M. Greuel, R. Muiyshondt, and P. T. Krein, "Design approaches to boundary controllers," in *Proc. IEEE Power Electron. Specialists Conf.*, 1997, pp. 672–678.
- [5] M. Carpita and M. Marchesoni, "Experimental study of a power conditioning system using sliding mode control," *IEEE Trans. Power Electron.*, vol. 11, no. 5, pp. 731–742, Sep. 1996.
- [6] B. J. Cardoso, A. F. Moreira, B. R. Menezes, and P. C. Cortizo, "Analysis of switching frequency reduction methods applied to sliding-mode controlled DC-DC converters," in *Proc. IEEE Appl. Power Electron. Conf. Expo.*, 1992, pp. 403–410.
- [7] C. H. Tso and J. C. Wu, "A ripple control buck regulator with fixed output frequency," *IEEE Power Electron. Lett.*, vol. 1, no. 3, pp. 61–63, Sep. 2003.

- [8] R. Miftakhutdinov, "Analysis of synchronous buck converter with hysteretic controller at high slew-rate load current transients," in *Proc. High Frequency Power Conv. Conf.*, 1999, pp. 55–69.
- [9] V. M. Nguyen and C. Q. Lee, "Tracking control of buck converter using sliding-mode with adaptive hysteresis," in *Proc. IEEE Power Electron. Specialists Conf.*, 1995, pp. 1086–1093.
- [10] A. S. Kislovski, R. Redl, and N. O. Sokal, *Dynamic Analysis of Switching-Mode DC-DC Converters*. New York: Van Nostrand, 1991.
- [11] K. K. S. Leung and H. S. H. Chung, "Derivation of a second-order switching surface in the boundary control of buck converters," *IEEE Power Electron. Lett.*, vol. 2, no. 2, pp. 63–67, Jun. 2004.
- [12] K. K. S. Leung and H. S. H. Chung, "Use of second-order switching surface in the boundary control of buck converter," in *Proc. IEEE Power Electron. Spec. Conf.*, Aachen, Germany, Jun. 2004, pp. 1587–1593.
- [13] K. K. S. Leung and H. S. H. Chung, "A Comparative study of the boundary control of buck converters using first- and second-order switching surfaces—Part I: continuous conduction mode," in *Proc. 36th IEEE Power Electron. Spec. Conf.*, Recife, Brazil, 2005, pp. 2133–2139.
- [14] S. C. Tan, Y. M. Lai, K. H. Cheung, and C. K. Tse, "On the practical design of a sliding mode voltage controlled buck converter," *IEEE Trans. Power Electron.*, vol. 20, no. 2, pp. 425–437, Mar. 2005.
- [15] J. J. E. Slotine and W. Li, "Sliding control," in *Applied Nonlinear Control*. Englewood Cliffs, NJ: Prentice-Hall, 1991, ch. 7.
- [16] N. Mohan, T. Undeland, and W. Robbins, *Power Electronics, Converters, Applications, and Design*. New York: Wiley, 2003.



Kelvin Ka-Sing Leung (S'03–M'06) received the B.Eng. (first class honors) and Ph.D. degrees in electronic engineering from the City University of Hong Kong, Kowloon, Hong Kong, in 2000 and 2005, respectively.

Currently, he is an Engineer at the MKS Instruments, Hong Kong. His research interests include dc-dc converter, switching surface control, and inverter applications.

Dr. Leung was the recipient of Chen Hsong Industrial Scholarships in 1999 and Chiap Hua Cheng's Foundation Scholarships, Shun Hing Education & Charity Fund Scholarship and IEE Prize in 2000 during his undergraduate studies.



Henry Shu-hung Chung (M'95–SM'03) received the B.Eng. and Ph.D. degrees in electrical engineering from The Hong Kong Polytechnic University, Hong Kong, in 1991 and 1994, respectively.

Since 1995, he has been with the City University of Hong Kong (CityU), Kowloon, Hong Kong, where currently, he is a Professor at the Department of Electronic Engineering and Chief Technical Officer of *e.Energy Technology Limited*—an associated company of CityU. He has authored six research book chapters, over 250 technical papers including

100 refereed journal papers in his research areas, and holds ten patents. His research interests include time- and frequency-domain analysis of power electronic circuits, switched-capacitor-based converters, random-switching techniques, control methods, digital audio amplifiers, soft-switching converters, and electronic ballast design.

Dr. Chung was IEEE student branch Counselor and Track Chair of the technical committee on power electronics circuits and power systems of IEEE Circuits and Systems Society in 1997–1998. He was the Associate Editor and Guest Editor of the IEEE TRANSACTIONS ON CIRCUITS AND SYSTEMS—PART I: FUNDAMENTAL THEORY AND APPLICATIONS in 1999–2003. Currently, he is an Associate Editor of the IEEE TRANSACTIONS ON POWER ELECTRONICS. He was awarded the Grand Applied Research Excellence Award in 2001 from the City University of Hong Kong.